IEEE Access
Multidisciplinary | Rapid Review | Open Access Journal

Received January 31, 2020, accepted February 13, 2020, date of publication February 17, 2020, date of current version March 2, 2020.

Digital Object Identifier 10.1109/ACCESS.2020.2974441

Generating Information-Diverse Microwave Speckle Patterns Inside a Room at a Single Frequency With a Dynamic Metasurface Aperture

OREN S. MIZRAHI[1], (Student Member, IEEE), MOHAMMADREZA F. IMANI[2], (Member, IEEE), JONAH N. GOLLUB[2], AND DAVID R. SMITH[2], (Senior Member, IEEE)

[1]Department of Electrical Engineering, California Institute of Technology, Pasadena, CA 91125, USA
[2]Center for Metamaterials and Integrated Plasmonics, Department of Electrical and Computer Engineering, Duke University, Durham, NC 27708, USA

Corresponding author: Oren S. Mizrahi (orensimonmizrahi@gmail.com)

The information, data, or work presented herein was funded in part by the Advanced Research Projects Agency-Energy (ARPA-E), US Department of Energy, under Award Number DE-AR0000937. The views and opinions of authors expressed herein do not necessarily state or reflect those of the Unites States Government or any agency thereof.

ABSTRACT We demonstrate that dynamic metasurface apertures (DMAs) are capable of generating a multitude of highly uncorrelated speckle patterns in a typical residential environment at a single frequency. We use a DMA implemented as an electrically-large cavity excited by a single port and loaded with many individually-addressable tunable metamaterial radiators. We placed such a DMA in one corner of a plywood-walled L-shape room transmitting microwave signals at 19 GHz as we changed the tuning states of the metamaterial radiators. In another corner, in the non-line-of-sight of the DMA, we conducted a scan of the field generated by the DMA. For comparison, we also performed a similar test where the DMA was replaced by a simple dipole antenna with fixed pattern but generating a signal that spanned $19 - 24$ GHz. Using singular value decomposition of the scanned data, we demonstrate that the DMA can generate a multitude of highly uncorrelated speckle patterns at a single frequency. In contrast, a dipole antenna with a fixed pattern can only generate such a highly uncorrelated set of patterns when operating over a large bandwidth. The experimental results of this paper suggest that DMAs can be used to capture a diversity of information at a single frequency which can be used for single frequency computational imaging systems, NLOS motion detection, gesture recognition systems, and more.

INDEX TERMS Antenna radiation patterns, radio frequency, sensors, antenna arrays, metamaterials.

I. INTRODUCTION

Computational imaging and sensing systems have recently gained traction due to their ability to retrieve information from a simplified hardware [1]–[9]. In this scheme, instead of relying on conventional techniques where there is a one-to-one relationship between points in a scene of interest and the measured data, the measurement process involves multiplexing information in a few simple data points and relying on computational techniques to retrieve desired information.

The associate editor coordinating the review of this manuscript and approving it for publication was Shah Nawaz Burokur.

In this framework, the simple hardware that can multiplex the information plays a key role. Multiplexing can be accomplished when the hardware is capable of *sensing* or *looking* at the target in diverse ways and incorporating these into a single measurement. To realize this condition, a large body of work - especially at microwave frequencies - have relied on using an array of antennas to generate the required diversity (e.g. MIMO systems [10], [11]) or frequency diversity (e.g. using multiple sub-channels in WiFi routers [12], [13], or frequency-diverse patterns [7]). Implementing spatial diversity using an array of antennas, while offering the desired performance, is cumbersome and expensive.

Frequency diversity can be even more crippling given the strict regulations on spectrum allotment and interference and the cost and complexity of large bandwidth hardware.

Another option to realize multiplexing is to use pattern diversity. This notion has seen great success in enabling computational microwave imaging at microwave frequencies over the last few years [14], [15]. In this scheme, a metasurface aperture acts as the central multiplexing element that generates pattern diversity. This aperture consists of an electrically large waveguide or a cavity that excites an array of metamaterial radiators. Each element is loaded with a tunable component and is addressed independently [16]. These tunable components allow for the selection of radiating (on) elements, paving the way for the generation of spatially distinct patterns that can multiplex the information content in the scene of interest. Using these DMAs, a variety of computational imaging scenarios have been reported in the literature [14], [15], [17]–[20]. A prominent example is [19] in which the multiplexing capabilities of the DMA allow for retrieving the scene information at a single frequency. In other words, the pattern diversity of the DMA was able to replace frequency or spatial diversity as is common in most computational imaging systems.

Inspired by successes in microwave imaging, some recent works have explored the extension of single frequency imaging to sensing and localization at a single frequency, relying solely on pattern diversity [21]–[23]. In these works, the DMA is used to form diverse patterns inside a disordered cavity, the physical equivalent of indoor environment at microwave frequencies. A simple dipole antenna is used to collect the scattered signal that has bounced several times inside the cavity. By examining the fluctuation of the received signal in this manner, the authors of [21], [23] showed the ability to detect motion even in non-line-of-sight areas and [22] demonstrated localization of non-cooperating objects.

While the results presented in [21]–[23] imply the ability of the DMA to realize pattern diversity inside a disordered cavity, this concept was never explicitly demonstrated. Furthermore, the setup used in [21], [22] are metallic cavities that are useful for *proof-of-concept* tests but have electromagnetic properties not generally applicable in real-life scenarios. In [23] sensing in a room with physically realistic parameters was explored, but only in simulation. In this work, we experimentally show that a DMA can enable pattern diversity inside a real-life scenario: a mock room enclosed in plywood walls rather than the metallic walls of [21], [22]. For comparison, we will show that the level of diversity among the patterns generated by the DMA at a single frequency is similar to that of a simple dipole antenna using frequency diversity over approximately 1 GHz of bandwidth.

II. EXPERIMENTAL SETUP

A. INDOOR TESTING CONFIGURATION

A life-size mock room aimed at emulating the conditions of a typical residential setting has been built for our experimental studies. This room, a top-view schematic of which is depicted in Fig. 1, is constructed using conventional 1.27 cm-thick plywood sheets with 5 × 10 cm beam reinforcements. The exterior of the room is covered with microwave absorbing foam to isolate the room from external microwave signals in our lab. The room layout is designed in an L shape to generate geometric complexity for both LOS and nLOS regions. Figure 2 depicts the constructed room and some of the spurious objects placed to emulate real-life scenarios. The ceiling of the room was partially (≈70%) covered by the same 1.27 cm-thick plywood sheets.

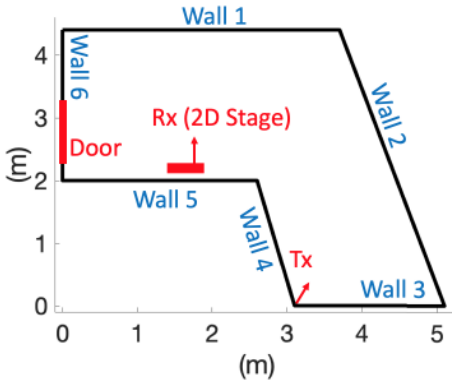

FIGURE 1. A top-down view of the mock room with key geometrical properties denoted.

B. DYNAMIC METASURFACE ANTENNA

The 2D DMA used in this paper is detailed in [24], [25]. Here, we briefly review its salient features relevant to the experiments at hand. This structure, shown in Fig. 3, consists of a double-sided copper clad substrate (60 mil thick Rogers 4003) with a via cage as a border. It is fed on one side by a coaxial connector which injects microwaves at $19 - 25$ GHz into the cavity. The other side is loaded with 96 metamaterial elements randomly distributed over the cavity. The choice of 96 elements was made to strike a compromise between the following concerns: 1. Too few elements would not have the desired potential for pattern diversity. 2. Too many elements would not fit in an aperture of this size. 3. 96 is a convenient number in that a single mask is coded in 12 bytes. Theoretically, any number of elements could have been used. The random distribution serves to prevent grating lobes and maximize the diversity of patterns compared to periodic patterns. Element positions were generated using a program that was tasked with generating a uniform random distribution with several constraints: 1. Inter-element distance could not be less than $\frac{\lambda}{2}$. 2. Elements could not be placed within $\frac{\lambda}{2}$ of the via cage or feed. These constraints maintained that a structure was physically feasible (enough provided space for decoupling stubs on the front side), that there was not undue coupling between elements, and that no elements would be coupled to ground through the vias or to the feed.

Each metamaterial element is loaded with a PIN diode **(Macom)** and is independently addressable. The overall size of the aperture is around 15 cm × 15cm. As microwaves

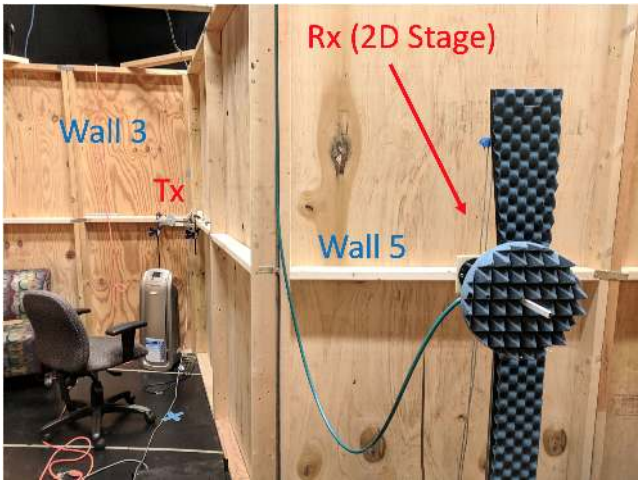

FIGURE 2. Interior view of room depicting the location of both antennas. Tx is shown on the left; Rx is shown on the 2D stage on the right.

bounce around inside the printed cavity, they leak through the metamaterial radiators that are tuned (by the PIN diode) to radiate. The resulting pattern, which is a superposition of the contributions from each metamaterial element, is an unconventional pattern with many lobes. By changing radiating and non-radiating elements using the PIN diodes, we can change the pattern and realize a set of spatially diverse patterns with simple, low-power tuning circuitry. In this paper, we refer to a unique configuration of on and off metamaterial radiators as a *mask* for brevity.

C. SCANNING SETUP

An extensive study of the patterns generated by this structure and its utility for computational imaging has been reported in [14]–[20], [24], [26]. The thorough investigation of which shows that the fabricated 2D DMA enables pattern diversity and multiplexing even at a single frequency in its radiative near field. Those conclusions can also be extended more or less to the LOS of the DMA placed in the room. In this work, we thus focus on its ability to realize pattern diversity in nLOS scenarios of a residential settings. Toward this goal, we scanned the field generated by the DMA in the room shown in Fig. 1: we placed the DMA at one corner of the room (see Fig. 1) while an open-ended waveguide antenna was mounted to a 2D linear stage, facing away from the DMA, in a nLOS region. The setup is shown in Fig. 2. The DMA is connected to Port 1 of a network analyzer and the receiving antenna was connected to Port 2. An Arduino is used to turn metamaterial elements on and off selectively.

The setup in Fig. 2 is similar to many real-life scenarios: an antenna in a corner transmitting a microwave signal which bounces around before arriving at a receiver. The phase accumulation along the trajectory is heavily dependent on the frequency of operation; as a result, many prior works have utilized this frequency dependence to probe different corners of the room. This idea manifests itself, for example, in WiFi-based sensing as *channel state information* (CSI).

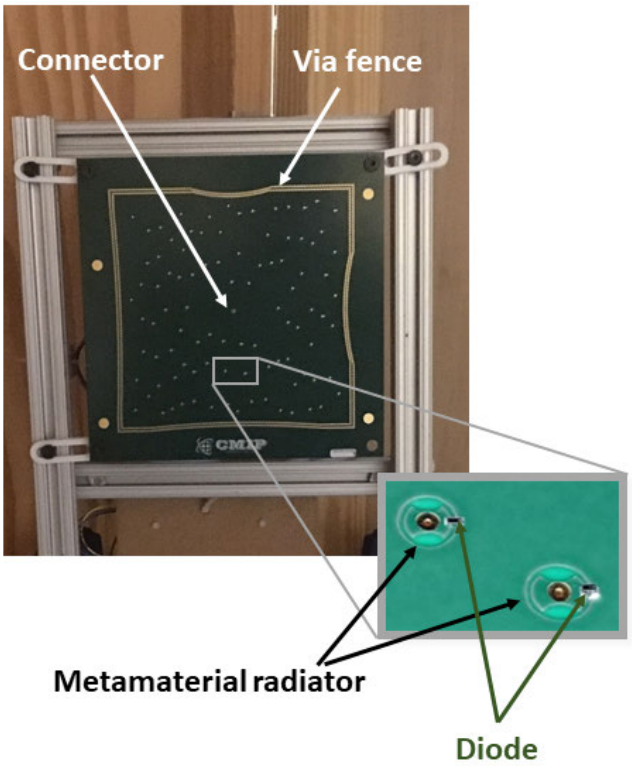

FIGURE 3. DMA mounted in the corner, serving as transmitter.

This scenario is also tested in our setup and is used to assess the ability of the DMA. Toward this goal, we also conducted a similar scan with the DMA replaced by a simple dipole antenna (an open-ended waveguide [27] in this case) with fixed pattern, but operating over a large (5 GHz) bandwidth. Our goal is to examine and compare the patterns generated in these two cases.

III. EXPERIMENTAL RESULTS

Using the setup discussed in the subsection II-C, we examine two cases: 1) when a simple dipole antenna (an open-ended waveguide antenna) acts as the transmitter and 2) when a DMA is used as the transmitter. In the first case, we scanned a receiving antenna over an area of 0.4 m x 0.4 m (sampling resolution of 5 mm) with 801 uniform frequency points (19-24 GHz). At each position and for each frequency point, we saved the scattering parameter between the transmitting and receiving antenna, $S_{21}^{\text{Dipole}}(x, y, m)$, where m indexes the frequency point. We then replaced the open-ended waveguide with the DMA and conducted a similar scan, this time only scanning at 19 GHz. At each point, we measured the signal for 200 masks, resulting in a matrix of the form $S_{21}^{\text{DMA}}(x, y, m)$, where m indexes the mask. The masks used consist of random distribution of *on* and *off* states, where 48 of the 96 elements were *on* in each mask.

We have plotted examples of the scanned data for different frequency points (for the dipole antenna) and different masks (for the DMA) in Fig. 4. In both cases, we can clearly discern speckle patterns formed as a result of the constructive

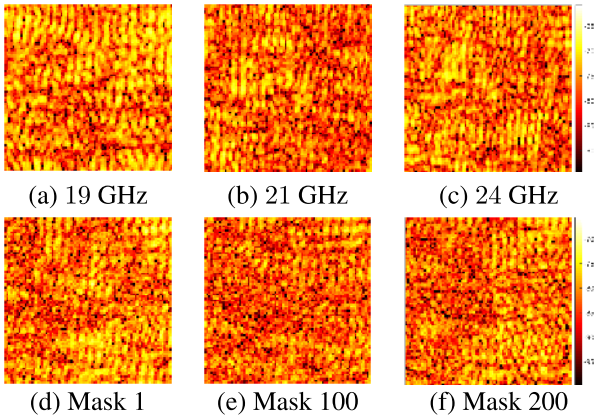

FIGURE 4. Scanned speckle patterns generated in NLOS region when (a)-(c) an OEWG and (d)-(f) a DMA act as the transmitter.

and destructive interference of the waves bouncing around inside the room. We also observe that the speckle patterns, as expected, change as a function of frequency for the dipole antenna. Interestingly, we also see substantial variation in the speckle patterns generated by the DMA as we use different masks.

A. SELF-SIMILARITY

To better assess the variation of the speckle patterns, we computed self-similarity matrices for both cases, defined as:

$$D_{ij} = \sum_x \sum_y |S_{21}(x, y, i) - S_{21}(x, y, j)| \tag{1}$$

$$\tilde{D} = 1 - \frac{D}{\max(D)}. \tag{2}$$

To ensure fair comparison, we down-sampled the frequency points of S_{21}^{Dipole} from 801 to 200 by picking out every 4^{th} frequency measurement and neglecting the one. The results of self-similarity calculation ($\tilde{D}$) are plotted in Fig. 5. As expected, $\tilde{D}_{ij} = 1, \forall(i = j)$. More remarkable is the relatively low magnitude of non-diagonal elements in this matrix. The mean of non-diagonal elements in $\tilde{D}$ was 0.34 for the dipole and 0.42 for the DMA. Relatively low similarity between non-diagonal elements gives us confidence that altering the measurement state (frequency or masks) of the system generates diverse speckle patterns; i.e. the destructive and constructive interference pattern formed inside the room changes.

B. SINGULAR VALUE DECOMPOSITION

Self-similarity examination does not, however, quantify the level of information diversity among patterns in the traditional sense. While the patterns may change visually between different frequency points or masks, it is more important to quantify how much new information is retrieved when patterns are changed. To do this, we examine the singular value decomposition (SVD) of the measured patterns. A relatively flat singular values indicates a high level of diversity between measurements. Meanwhile, a quickly-decaying SVD curve indicates a low-rank system with a high degree of correlation

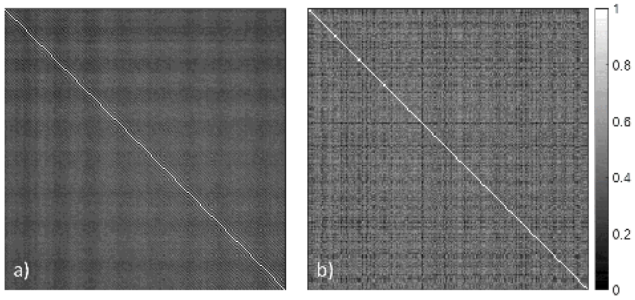

FIGURE 5. Self similarity matrices, $\tilde{D}$, for the speckle patterns generated using a) a dipole antenna and b) a DMA.

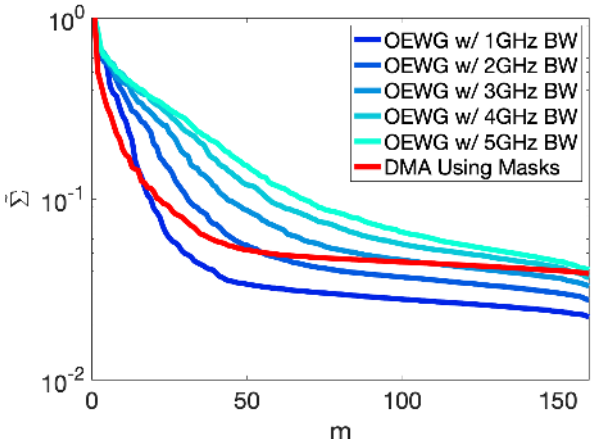

FIGURE 6. Normalized SVD for DMA modulating over masks and a dipole antenna sweeping over two different bandwidths.

between patterns. To compute the singular values for a system of 2D scans, we recast the scanned data into a flattened 2D matrix, amalgamating the horizontal and vertical dimensions into a single "spatial" dimension. This new 2D data matrix is given by $\widetilde{S}_{21}(r, m) \in \mathbb{C}^{N_x N_y \times M}$, where $r = x + N_x(y - 1)$ indexes over all positions, and N_x and N_y are the total number of pixels in the horizontal and vertical directions, respectively.

For the dipole case, we generate an SVD curve for 5 different bandwidths, where in each case, we down-sampled to 160 frequency points. For example, the data for 5 GHz was sampled every 5 frequency points, with the last data point neglected. In all cases, we have $\widetilde{S}_{21}(r, m) \in \mathbb{C}^{N_x N_y \times 160}$. An equal number of evenly-spaced measurements facilitates a fair comparison between the frequency-diverse data and the DMA data. The singular value decomposition was computed in MATLAB and is given below:

$$\widetilde{S}_{21} = U \Sigma V^{\dagger} \tag{3}$$

$$\widetilde{\Sigma} = \frac{\Sigma}{\max(\Sigma)} \tag{4}$$

where $\Sigma = \text{diag}(\sigma_1, \sigma_2, \ldots, \sigma_m)$ is a diagonal matrix containing sorted singular values of $\widetilde{S}_{21}$ and $V^{\dagger}$ is the conjugate transpose of the matrix V. We have plotted the normalized singular value spectrum, $\widetilde{\Sigma}$, for 5 different bandwidths and for the DMA in Fig. 6.

Our first observation is that as we decrease the bandwidth of operation for the dipole antenna, the correlation among

speckle patterns increases. We can also see that the level of information diversity provided by the 160 masks of the DMA is on par with using $\approx$ 1 GHz of bandwidth on a fixed-pattern dipole antenna when using few measurements ($m \leq 50$). However, when looking at the contribution of the later measurements ($m \geq 100$), we can see that the DMA has higher singular values than most bandwidths and has a flatter curve overall.

In short, when using a SVD to quantify the relative contribution of each measurement to the basis, a DMA can retrieve the same amount of information as would be possible using a conventional system composed of a fixed-pattern antenna with 1 GHz of bandwidth. DMA spatial diversity can thus replace the frequency diversity obtained by using 1 GHz of bandwidth ($\approx 5\%$ fractional bandwidth).

It is worth noting that spatial diversity obtained by DMA can be attributed to its electrically large size. In a similar manner, WiFi systems can also use several antennae (formed in a MIMO configuration), and reduce reliance on bandwidth. The DMA replaces the configuration complexity of building such a system with the convenience a single-port device simply by switching masks.

It is important to note that we have reported normalized singular values. The average power radiated by the DMA is lower than that of the dipole antenna; this is expected given that we have not optimized the DMA for efficiency. Lower efficiency can easily be compensated for by increasing the power of the source or increasing the dynamic range of the receiver; because we operate at a single frequency, improving dynamic range or increasing power can be realized with minimal increase in the complexity or cost of the RF hardware.

C. EFFECTIVE RANK

Looking at the SVD curves can be useful for tracking the increase in correlation among patterns as we include more in our measurement basis. However, it may be more useful to consolidate this data into a single number which captures the dimension of the pattern basis. Traditionally, this value is the *rank* of the measurement matrix. However, traditional calculations of rank do not apply well here. Because our measurements are complex and noisy, it is unlikely that any pattern is *exactly* the linear combination of any of the other patterns. As a result, when we used the traditional method of computing rank (e.g. as it is done using MATLAB rank function), all 6 basis matrices which correspond to $\widetilde{S}_{21}(r, m)$ - 5 for OEWG bandwidths and 1 DMA - had full rank of 160.

Instead, we used a measure of *effective rank*, originally conceived in [28] which has been used as a measure of the quantity of information diversity in MIMO communication [29]. The expression for the effective rank of a matrix, $A \in \mathbb{C}^{P\times Q}$, is given in Equation 2 in [29] and has been replicated below:

$$R_{\text{eff}}(A) = \exp\left[-\sum_{i=1}^{I} \sigma_i' \ln(\sigma_i')\right] \tag{5}$$

TABLE 1. Rank and effective rank for 6 pattern matrices.

Antenna	BW (GHz)	R	R_{eff}
Dipole	1	160	71.78
Dipole	2	160	85.53
Dipole	3	160	94.69
Dipole	4	160	101.63
Dipole	5	160	107.35
DMA	0	160	108.06

where $I = \min(P, Q)$ and $\sigma_i' = \frac{\sigma_i}{\sum_{i=1}^{I}\sigma_i}$ are the normalized singular values of A.

We applied this method toward the pattern matrices, $\widetilde{S}_{21}(r, m)$, to determine the degree of linear independence for each of our pattern bases. Table 1 lists our results. For reference, we listed the traditional rank, R, for each matrix.

Examining effective rank listed in Table 1, we should note that when a matrix $A \in \mathbb{C}^{P\times Q}$ is full rank ($R = \min(P, Q)$), each vector is independent of all other vectors and contributes a new dimension to the basis. In such a scenario, additional vectors (beyond the rank) contribute no new information. $R_{\text{eff}} < R$ *does not* imply that $R - R_{\text{eff}}$ vectors in the pattern basis are "useless" linear combinations of other vectors. Because R_{eff} uses the SVD to estimate the dimension of the pattern basis, we must recognize that all vectors in the pattern basis contribute new information. Instead, our effective rank measurement is an attempt to gauge how much information is captured by our 160 measurements. $R_{\text{eff}} = 71.78$ (for the case of a dipole antenna with 1GHz of bandwidth, for example) means that we have captured slightly less than half of the information we could have, given redundancy and correlation in our measurement matrix. In the context of image classification, for example, this value can be helpful in deciding how many measurements one needs to uniquely identify one of N possible options.

Looking at the trend of R_{eff} for the dipole antennas, we can clearly see an increase in the effective rank of our measurement matrix as our bandwidth increases. Although all 5 measurement matrices pertinent to the dipole operating over a bandwidth contain 160 measurements, the smaller bandwidth cases have more linearly dependent measurements because they are closer in frequency. Conversely, there is more information diversity and more linear independence in the patterns generated over 5GHz.

Impressively, despite utilizing 0 bandwidth, the DMA ranks *highest* among all 6 bases in terms of the linear independence between measurements in the measurement matrix. This means that we are capable of generating and/or capturing more information diversity with a DMA switching masks at a single frequency than a dipole antenna with 5GHz of bandwidth.

IV. CONCLUSION

Thus, we have demonstrated an ability to generate information-diverse speckle patterns at a single frequency with a DMA in a residential setting. Firstly, we used self-similarity matrices to demonstrate that the patterns are

visually distinct in the sense that points of constructive interference and destructive interference change when the pattern changes. Secondly, we plotted SVD curves for our DMA at a single frequency and overlaid curves for a conventional antenna with $1-5$ GHz of bandwidth. These curves demonstrate that the DMA captures new information with each subsequent radiation pattern and the degree to which it does so is on par with a normal antenna using $1-2$ GHz of bandwidth. The DMA's SVD curve is also flatter overall than the conventional antenna curves, indicating that the information contribution of subsequent measurements is greater for the DMA. Finally, we quantified the degree of linear independence of patterns by using a measurement of effective rank. Despite operating with no bandwidth, the DMA had a higher effective rank than a conventional antenna operating with 5 GHz of bandwidth.

These results indicate the plausibility of using a DMA in the context of computational imaging or sensing. For example, we can perform single-pixel, single-frequency imaging using M masks. Each image would consist of a $1 \times M$ vector. To perform gesture recognition, one could train a neural network (NN) to classify these vectors. Because we know our measurement basis has an effective dimension on par with M, we have confidence that the image contains enough unique information for the CNN to capitalize on for automated classification.

Moreover, the potential to generate information-diverse speckle patterns makes the DMA an excellent candidate for sensing purposes, for example in motion detection systems which demand high room coverage and suffer in complex and NLOS geometries. We plan to explore these applications and more in our future work.

ACKNOLWEDGMENT

This work was completed when O.S.M. was with the Center for Metamaterials and Integrated Plasmonics, Duke University.

REFERENCES

[1] R. Fergus, A. Torralba, and W. T. Freeman, "Random lens imaging," MIT Comput. Sci. Artif. Intell. Lab., Cambridge, MA, USA, Tech. Rep., 2006, vol. 58, no. 2006, p. 1.

[2] D. J. Brady, K. Choi, D. L. Marks, R. Horisaki, and S. Lim, "Compressive holography," *Opt. Express*, vol. 17, no. 15, pp. 13040–13049, 2009.

[3] D. J. Brady, *Optical Imaging and Spectroscopy*. Hoboken, NJ, USA: Wiley, 2009.

[4] J. Hunt, T. Driscoll, A. Mrozack, G. Lipworth, M. Reynolds, D. Brady, and D. R. Smith, "Metamaterial apertures for computational imaging," *Science*, vol. 339, no. 6117, pp. 310–313, Jan. 2013.

[5] A. Liutkus, D. Martina, S. Popoff, G. Chardon, O. Katz, G. Lerosey, S. Gigan, L. Daudet, and I. Carron, "Imaging with nature: Compressive imaging using a multiply scattering medium," *Sci. Rep.*, vol. 4, no. 1, p. 5552, May 2015.

[6] O. Katz, P. Heidmann, M. Fink, and S. Gigan, "Non-invasive single-shot imaging through scattering layers and around corners via speckle correlations," *Nature Photon.*, vol. 8, no. 10, pp. 784–790, Oct. 2014.

[7] J. N. Gollub, O. Yurduseven, K. P. Trofatter, D. Arnitz, M. F. Imani, T. Sleasman, M. Boyarsky, A. Rose, A. Pedross-Engel, H. Odabasi, T. Zvolensky, G. Lipworth, D. Brady, D. L. Marks, M. S. Reynolds, and D. R. Smith, "Large metasurface aperture for millimeter wave computational imaging at the human-scale," *Sci. Rep.*, vol. 7, no. 1, p. 42650, May 2017.

[8] L.-H. Yeh, L. Tian, and L. Waller, "Structured illumination microscopy with unknown patterns and a statistical prior," *Biomed. Opt. Express*, vol. 8, no. 2, p. 695, Feb. 2017.

[9] J. N. Mait, G. W. Euliss, and R. A. Athale, "Computational imaging," *Adv. Opt. Photon.*, vol. 10, no. 2, pp. 409–483, 2018.

[10] G. Krieger, "MIMO-SAR: Opportunities and pitfalls," *IEEE Trans. Geosci. Remote Sens.*, vol. 52, no. 5, pp. 2628–2645, May 2014.

[11] S. S. Ahmed, *Electronic Microwave Imaging With Planar Multistatic Arrays*. Berlin, Germany: Logos Verlag Berlin GmbH, 2014.

[12] C. Wu, Z. Yang, Z. Zhou, X. Liu, Y. Liu, and J. Cao, "Non-invasive detection of moving and stationary human with WiFi," *IEEE J. Sel. Areas Commun.*, vol. 33, no. 11, pp. 2329–2342, Nov. 2015.

[13] B. Wang, Q. Xu, C. Chen, F. Zhang, and K. J. R. Liu, "The promise of radio analytics: A future paradigm of wireless positioning, tracking, and sensing," *IEEE Signal Process. Mag.*, vol. 35, no. 3, pp. 59–80, May 2018.

[14] T. Sleasman, M. F. Imani, J. N. Gollub, and D. R. Smith, "Dynamic metamaterial aperture for microwave imaging," *Appl. Phys. Lett.*, vol. 107, no. 20, Nov. 2015, Art. no. 204104.

[15] T. Sleasman, M. F. Imani, J. N. Gollub, and D. R. Smith, "Microwave imaging using a disordered cavity with a dynamically tunable impedance surface," *Phys. Rev. A, Gen. Phys.*, vol. 6, no. 5, Nov. 2016, Art. no. 054019.

[16] T. Sleasman, M. F. Imani, W. Xu, J. Hunt, T. Driscoll, M. S. Reynolds, and D. R. Smith, "Waveguide-fed tunable metamaterial element for dynamic apertures," *IEEE Antennas Wireless Propag. Lett.*, vol. 15, pp. 606–609, 2016.

[17] T. Sleasman, M. Boyarsky, M. F. Imani, J. N. Gollub, and D. R. Smith, "Design considerations for a dynamic metamaterial aperture for computational imaging at microwave frequencies," *J. Opt. Soc. Amer. B, Opt. Phys.*, vol. 33, no. 6, p. 1098, Jun. 2016.

[18] T. Sleasman, M. Boyarsky, L. Pulido-Mancera, T. Fromenteze, M. F. Imani, M. S. Reynolds, and D. R. Smith, "Experimental synthetic aperture radar with dynamic metasurfaces," *IEEE Trans. Antennas Propag.*, vol. 65, no. 12, pp. 6864–6877, Dec. 2017.

[19] T. Sleasman, M. Boyarsky, M. F. Imani, T. Fromenteze, J. N. Gollub, and D. R. Smith, "Single-frequency microwave imaging with dynamic metasurface apertures," *J. Opt. Soc. Amer. B, Opt. Phys.*, vol. 34, no. 8, pp. 1713–1726, Aug. 2017.

[20] A. V. Diebold, M. F. Imani, T. Sleasman, and D. R. Smith, "Phaseless computational ghost imaging at microwave frequencies using a dynamic metasurface aperture," *Appl. Opt.*, vol. 57, no. 9, pp. 2142–2149, Mar. 2018.

[21] P. del Hougne, M. F. Imani, T. Sleasman, J. N. Gollub, M. Fink, G. Lerosey, and D. R. Smith, "Dynamic metasurface aperture as smart around-the-corner motion detector," *Sci. Rep.*, vol. 8, no. 1, Dec. 2018, Art. no. 6536.

[22] P. del Hougne, M. F. Imani, M. Fink, D. R. Smith, and G. Lerosey, "Precise localization of multiple noncooperative objects in a disordered cavity by wave front shaping," *Phys. Rev. Lett.*, vol. 121, no. 6, Aug. 2018, Art. no. 063901.

[23] O. S. Mizrahi, M. F. Imani, K. P. Trofatter, J. N. Gollub, and D. R. Smith, "2D ray tracing analysis of a dynamic metasurface antenna as a smart motion detector," *IEEE Access*, vol. 7, pp. 159674–159687, 2019.

[24] M. F. Imani, T. Sleasman, and D. R. Smith, "Two-dimensional dynamic metasurface apertures for computational microwave imaging," *IEEE Antennas Wireless Propag. Lett.*, vol. 17, no. 12, pp. 2299–2303, Dec. 2018.

[25] T. Sleasman, M. F. Imani, A. V. Diebold, M. Boyarsky, K. P. Trofatter, and D. R. Smith, "Implementation and characterization of a two-dimensional printed circuit dynamic metasurface aperture for computational microwave imaging," 2019, *arXiv:1911.08952*. [Online]. Available: http://arxiv.org/abs/1911.08952

[26] T. Fromenteze, X. Liu, M. Boyarsky, J. Gollub, and D. R. Smith, "Phaseless computational imaging with a radiating metasurface," *Opt. Express*, vol. 24, no. 15, pp. 16760–16776, Jul. 2016.

[27] A. Yaghjian, "Approximate formulas for the far field and gain of open-ended rectangular waveguide," *IEEE Trans. Antennas Propag.*, vol. AP-32, no. 4, pp. 378–384, Apr. 1984.

[28] O. Roy and M. Vetterli, "The effective rank: A measure of effective dimensionality," in *Proc. 15th Eur. Signal Process. Conf.*, 2007, pp. 606–610.
[29] P. del Hougne, M. Fink, and G. Lerosey, "Optimally diverse communication channels in disordered environments with tuned randomness," *Nature Electron.*, vol. 2, no. 1, pp. 36–41, Jan. 2019.

OREN S. MIZRAHI (Student Member, IEEE) received the B.S.E. degree in biomedical engineering and the B.S.E. degree in electrical & computer engineering from Duke University, Durham, NC, USA, in 2019. He is currently pursuing the Ph.D. degree in electrical engineering with the California Institute of Technology, Pasadena, CA, USA. He joined the Center for Metamaterials and Integrated Plasmonics, Duke University, in 2018, as an undergraduate Pratt Fellow. From 2018 to 2019, he worked toward the development of metasurface-based sensing systems.

MOHAMMADREZA F. IMANI (Member, IEEE) received the B.S.E. degree in electrical engineering from the Sharif University of Technology, Tehran, Iran, in 2007, and the M.S.E. and Ph.D. degrees in electrical engineering from the University of Michigan, Ann Arbor, MI, USA, in 2010 and 2013, respectively.

From 2014 to 2018, he served as a Postdoctoral Associate with the Department of Electrical and Computer Engineering, Duke University, Durham, NC, USA, where he is currently a Research Scientist. He has authored and coauthored more than 70 journal and conference papers and holds 1 granted and 5 pending patent applications. His researches include analytical and applied electromagnetics, metamaterials and metasurfaces, microwave imaging and sensing, wireless power transfer, antenna analysis and synthesis, and MIMO communication systems.

JONAH N. GOLLUB received the B.A. degree in physics from the Reed College, in 2000, and the Ph.D. degree in physics from the University of California at San Diego, San Diego, in 2009. His thesis work covered a variety of metamaterial focused topics, including the hybridization of metamaterials with magnetic materials and the demonstration of magnetic surface plasmon polaritons on metamaterials. From 2010 to 2013, he worked as a Lead Modeling and Simulation Scientist at a startup company developing surface metamaterials, with applications for imaging and biological detection under DARPA, MDA, Army, and NSF funded efforts. In 2013, he joined Duke University as a Research Scientist to focus on the development of a real-time millimeter wave imaging system utilizing frequency diverse metasurface antennas and computational imaging techniques.

DAVID R. SMITH (Senior Member, IEEE) received the B.S. and Ph.D. degrees in physics from the University of California at San Diego, San Diego, CA, USA, in 1988 and 1994, respectively. He is currently the James B. Duke Professor of electrical and computer engineering with Duke University and the Director of the Center for Metamaterials and Integrated Plasmonics. He has provided key experimental demonstrations in the metamaterials field, including the first demonstration of a negative index metamaterial, in 2000, and the first demonstration of a metamaterial invisibility cloak, in 2006. His research interests include the theory, simulation, and characterization of unique electromagnetic structures, including photonic crystals and metamaterials, and applications of such materials. He was elected as a Fellow of the National Academy of Inventors, in 2016. He was a co-recipient of the Descartes Scientific Research Prize awarded by the European Union, in 2005, and the James C. McGroddy Prize for New Materials, awarded by the American Physical Society, in 2013. Since 2009, he has been listed as a Highly Cited Researcher by Clarivate Analytics in the field of physics.